

## BeppoSAX MEASUREMENTS OF THE BRIGHT GAMMA-RAY BURST 010222

J. J. M. IN 'T ZAND,<sup>1,2</sup> L. KUIPER,<sup>2</sup> L. AMATI,<sup>3</sup> L. A. ANTONELLI,<sup>4,5</sup> R. C. BUTLER,<sup>3</sup> E. COSTA,<sup>6</sup> M. FEROCI,<sup>6</sup>  
F. FRONTERA,<sup>3,7</sup> G. GANDOLFI,<sup>6</sup> C. GUIDORZI,<sup>7</sup> J. HEISE,<sup>2</sup> R. G. KAPTEIN,<sup>2,8</sup> E. KUULKERS,<sup>1,2</sup> L. NICASTRO,<sup>9</sup> L. PIRO,<sup>6</sup>  
P. SOFFITTA,<sup>6</sup> AND M. TAVANI<sup>10,11</sup>

Received 2001 April 13; accepted 2001 June 5

### ABSTRACT

We analyze the *BeppoSAX* measurements of the prompt and afterglow emission of the  $\gamma$ -ray burst GRB 010222. Among 45 GRBs detected with the Wide Field Cameras on *BeppoSAX*, the 40–700 keV fluence of  $(9.3 \pm 0.3) \times 10^{-5}$  ergs  $\text{cm}^{-2}$  is only surpassed by GRB 990123. In terms of the isotropic 20–2000 keV energy output of  $7.8 \times 10^{53}$  ergs, it ranks third of all GRBs with measured distances. Since this burst is so bright, the data provide complete and valuable coverage up to 65 hr after the event, except for a gap between 3.5 and 8.0 hr. The 2–10 keV flux history shows clear signs of a break, which is consistent with a break seen in the optical, and provides supporting evidence for the achromatic nature of the break. An explanation for the break in the context of a collimated expansion is not straightforward. Rather, a model is favored whereby the fireball is braked to the nonrelativistic regime quickly (within a fraction of day) by a dense ( $\sim 10^6 \text{ cm}^{-3}$ ) circumburst medium. This implies that, after a mild beaming correction, GRB 010222 may be the most energetic burst observed thus far. The X-ray decay index after the break is  $1.33 \pm 0.04$ , the spectral index  $0.97 \pm 0.05$ . The decay is, with unprecedented accuracy, identical to that observed in the optical.

*Subject headings:* gamma rays: bursts — X-rays: general

### 1. INTRODUCTION

In its nearly 5 year mission up to 2001 March, the Wide Field Cameras (WFCs) and Gamma-Ray Burst Monitor (GRBM) on the *BeppoSAX* platform simultaneously detected 45  $\gamma$ -ray bursts (GRBs) that were analyzed in near-real time. An increasing number of bursts are sampled at the high end of the peak flux distribution. In this paper we discuss GRB 010222, which is the most energetic burst detected after GRB 990123.

The GRBM was triggered by GRB 010222 on 2001 February 22.3073484 UT. Simultaneously, WFC unit 1 detected this burst at an off-axis angle of  $15^\circ$ . The WFC detection is of high statistical significance, and the burst could be localized within 2.5 (Piro 2001). An alert message was distributed 3.2 hr after the burst, and follow-up studies were quick, thanks to the favorable declination and timing of the burst. A  $V = 18$  optical counterpart was publicly announced within 4.4 hr after the burst (Henden 2001a, 2001b); a radio

counterpart at 22 GHz within 7.7 hr (Berger & Frail 2001); and detections followed in the *R* band (Stanek et al. 2001b), near-infrared (Di Paola et al. 2001), and at sub-mm wavelengths (Fich et al. 2001). Remarkably, the first report of a redshift appeared within only 11.4 hr (Garnavich et al. 2001a). Later studies (Jha et al. 2001a, 2001b ; Bloom et al. 2001a ) revealed absorption systems at three different redshifts, with  $z = 1.477$  the largest. Jha et al. (2001a) argue that the  $z = 1.477$  system is actually from the host galaxy.

We here present all GRB 010222 measurements that were obtained with *BeppoSAX* instruments. These pertain to the burst itself (in X-rays and  $\gamma$ -rays) and the X-ray afterglow. Since the burst is so bright, the statistical quality of these data is high and allows for a sensitive study of various aspects of this burst. We discuss the radiation output of the burst and the evidence for a dense circumburst environment.

### 2. THE BURST EVENT

The burst event was measured with two instruments on board *BeppoSAX* (Boella et al. 1997b). The GRBM (Amati et al. 1997; Feroci et al. 1997) comprises four lateral shields of the Phoswich Detector System (PDS; Frontera et al. 1997) and has a bandpass of 40 to 700 keV. The normal directions of two shields are each coaligned with the viewing direction of a WFC unit. The WFCs (Jager et al. 1997) consist of two identical coded aperture cameras, each with a field of view of  $40^\circ \times 40^\circ$  full-width to zero response and an angular resolution of about  $5'$ . The bandpass is 2 to 28 keV.

In Figure 1, the time profile of the burst is shown in various bandpasses. The  $\gamma$ -ray light curve consists of seven clear pulses over a  $\approx 130$  s time interval, with recursions to almost the quiescent level in between. The GRBM triggered on the second pulse. At a resolution of 7.8125 ms (not shown) the main peak shows five sub-pulses. The peak flux is  $30 \pm 5\%$  higher at 62.5 ms than at 1 s time resolution.

<sup>1</sup> Astronomical Institute, Utrecht University, P.O. Box 80 000, 3508 TA Utrecht, the Netherlands.

<sup>2</sup> Space Research Organization Netherlands, Sorbonnelaan 2, 3584 CA Utrecht, the Netherlands; jeanz@sron.nl.

<sup>3</sup> Istituto di Tecnologie e Studio delle Radiazioni Extraterrestri (CNR), Via Gobetti 101, 40129 Bologna, Italy.

<sup>4</sup> Osservatorio Astronomico di Roma, Via Frascati 33, 00040 Monteporzio Catone, Italy.

<sup>5</sup> *BeppoSAX* Science Data Center, Via Corcolle 19, 00131 Rome, Italy.

<sup>6</sup> Istituto di Astrofisica Spaziale (CNR), 00133 Rome, Italy.

<sup>7</sup> Dipartimento Fisica, Università di Ferrara, Via Paradiso 12, 44100 Ferrara, Italy.

<sup>8</sup> *BeppoSAX* Scientific Operation Center, Via Corcolle 19, 00131 Rome, Italy.

<sup>9</sup> Istituto Fisica Cosmica e Applicazioni all'Informatica (CNR), Via Ugo La Malfa 153, 90146 Palermo, Italy.

<sup>10</sup> Istituto Fisica Cosmica e Tecnologie Relative (CNR), Via Bassini 15, 20133 Milan, Italy.

<sup>11</sup> Columbia Astrophysics Laboratory, Columbia University, New York, NY 10027.

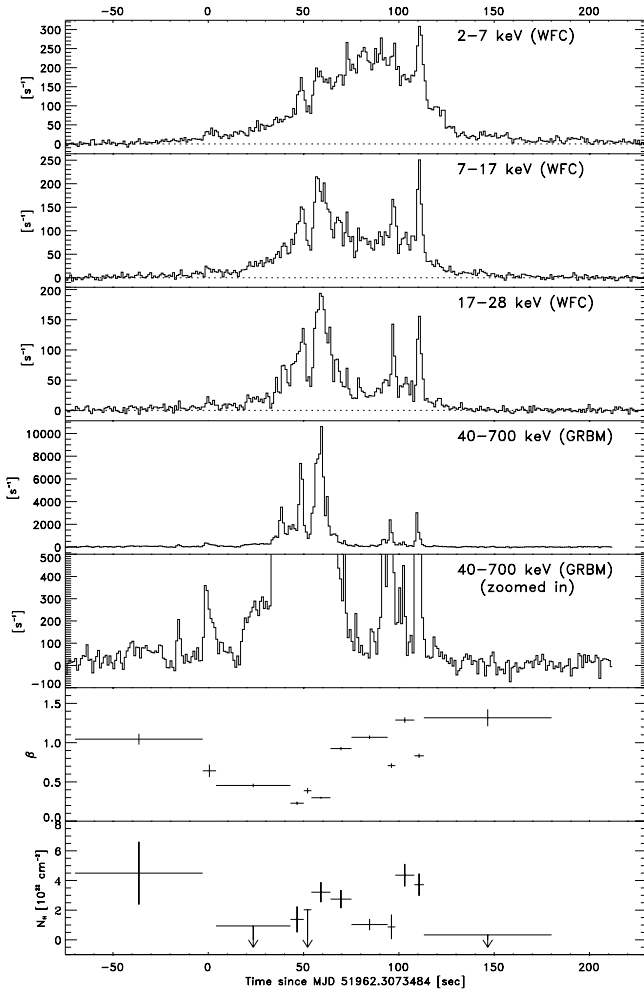


FIG. 1.—Time history of the burst itself as seen with WFC and GRBM, at a time resolution of 1 s. The two lower panels present the evolution of the power-law index  $\beta$  and absorption column  $N_H$  as simultaneously determined from WFC and two-channel GRBM data, except for the last data point, which did not contain a significant GRBM signal. Upper limits for  $N_H$  are  $1\sigma$  values.

The Fourier power spectrum shows no narrow features. When carefully investigating the  $\gamma$ -ray flux before the first pulse (Fig. 1, *fifth panel*), it shows a slight increase at 40 s before the trigger time, with rates going up to about  $100\text{ s}^{-1}$  (or 1% of the peak rate). The X-ray light curve starts off at approximately the same moment. It is characterized by a slow rise, which persists during the first  $\gamma$ -ray pulses. This behavior is reminiscent of other bursts, some of which have apparent X-ray precursor activity (e.g., In ’t Zand et al. 1999). Perhaps in some of those cases we are simply missing the weak  $\gamma$ -ray emission because the flux does not exceed the detection threshold. Noteworthy also is that the X-radiation continues for some 150 s after the cessation of the  $\gamma$ -radiation. Both the X-ray and  $\gamma$ -ray light curves show strong spectral evolution.

In Table 1 we list the duration, peak flux, and fluence of the prompt emission. In many respects, GRB 010222 ranks in the top three of GRBs that were detected with WFC. In terms of 2–28 keV peak flux, GRB 010222 ranks second after GRB 990712 (by a factor of 1.8; Frontera et al. 2001). The X-ray duration of  $\approx 280$  s is among the longest measured with WFC, together with GRB 980519 (250 s;

TABLE 1

BASIC PARAMETERS OF THE PROMPT EMISSION.

Parameter	Bandpass (keV)	Value
Duration (s) .....	2–28	$\approx 280$
	40–700	$\approx 170$
Peak flux ( $\text{ergs s}^{-1} \text{cm}^{-2}$ ) .....	2–10	$(2.1 \pm 0.2) \times 10^{-7}$
	2–28	$(4.6 \pm 0.5) \times 10^{-7}$
	40–700	$(8.6 \pm 0.2) \times 10^{-6}$
	50–300	$(3.6 \pm 0.4) \times 10^{-6}$
Peak flux ( $\text{photons s}^{-1} \text{cm}^{-2}$ ).....	50–300	$19 \pm 2$
Fluence ( $\text{ergs cm}^{-2}$ ) .....	2–10	$(1.03 \pm 0.03) \times 10^{-5}$
	2–28	$(2.20 \pm 0.06) \times 10^{-5}$
	40–700	$(9.25 \pm 0.28) \times 10^{-5}$
	2–700	$(1.20 \pm 0.03) \times 10^{-4}$
	50–300	$(4.88 \pm 0.13) \times 10^{-5}$

In ’t Zand et al. 1999), GRB 981226 (250 s; Frontera et al. 2000), and GRB 990907 (230 s). The combination of longevity and brightness makes this burst number one in X-ray fluence: its fluence is 3 times larger than the next burst in line (GRB 990712). In 40–700 keV peak flux, it ranks third after GRB 000210 (Stornelli et al. 2000) and GRB 990123 (Feroci et al. 1999), and in fluence it ranks second after GRB 990123. The 50–300 keV burst fluence places it in the top 1.3% of the BATSE burst samples and the 50–300 keV peak photon flux in the top 2.5%.

The GRBM continuously samples 256 channel spectra every 128 s between 40 and 700 keV. 240 of these channels are well calibrated, roughly between 50 and 650 keV. The phasing of the accumulation timing is arbitrary. GRB 010222 is covered by two 128 s accumulation intervals that meet at 37 s after the trigger time. In Figure 2 we show these spectra, combined with the appropriate WFC data. There is evidence for a break at 210 keV and for a low-energy cutoff that may be fitted with absorption due to cold interstellar matter. The GRBM also provides photon rates at 1 s resolution in 40–700 keV and greater than 100 keV. If these data and the WFC data are resolved in 12 time intervals (see bottom panels of Figure 1), and an absorbed power law is fitted,<sup>12</sup> where the index is left free over all 12 intervals, while  $N_H$  is a single free parameter over all intervals,  $\beta$  varies between 0.0 and 1.5, while  $N_H = (1.7 \pm 0.2) \times 10^{22} \text{ cm}^{-2}$ . The values for  $\beta$  are in good agreement with the shock synchrotron model put forward by Tavani (1996). If  $N_H$  is left free,  $\chi^2_\nu$  improves significantly from 0.943 (358 dof) to 0.931 (348 dof). An  $f$ -test shows a negligible chance probability.  $N_H$  varies between non-detections with  $3\sigma$  upper limits as small as  $1.0 \times 10^{22} \text{ cm}^{-2}$  (for the last interval) to a peak of  $4 \times 10^{22} \text{ cm}^{-2}$  (see Fig. 1). Note that  $N_H$  for the Galactic absorption in the direction of the burst is  $1.6 \times 10^{20} \text{ cm}^{-2}$  according to an interpolation of the maps published by Dickey & Lockman (1990).

The WFC observation on this field was from 17.8 hr before the burst till 3.5 hr afterward. A total of 16.9 ks of net exposure time was accumulated. We could not find any

<sup>12</sup> Formulated by  $F(E) \sim \exp(-N_H \sigma(E)) E^{-\beta} \text{ keV s}^{-1} \text{ cm}^{-2} \text{ keV}^{-1}$ , where  $\sigma(E)$  is the cross section as a function of photon energy  $E$  for cold interstellar matter of cosmic abundances according to the model by Morrison & McCammon (1983),  $N_H$  is the hydrogen column density, and  $\beta$  is the energy index.

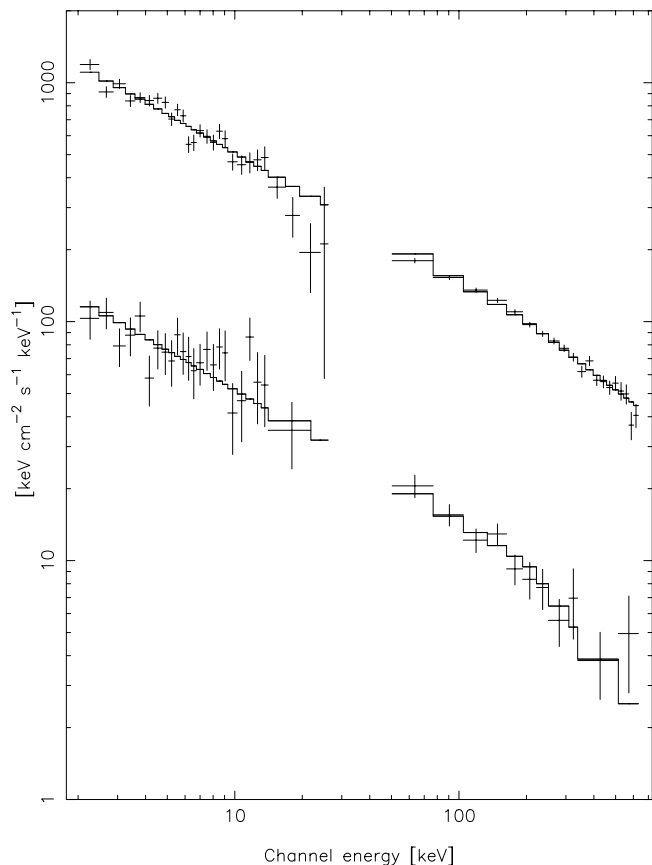


FIG. 2.—Combined WFC and GRBM spectra for intervals  $-91/+37$  (lower curve) and  $+37/+165$  s (upper curve) after the trigger time. The solid lines indicate the best-fit absorbed broken power-law function with the same absorption and break energy in both cases. The  $\chi^2_\nu = 1.346$  for  $\nu = 88$  dof, the break energy is  $210 \pm 30$  keV. There is no improvement in the fit if the break energy is left free in each interval. The spectral index  $\beta$  is  $0.56 \pm 0.02$  below and  $1.3 \pm 0.3$  above the break for the lower curve and  $0.543 \pm 0.007$  and  $0.72 \pm 0.04$ , respectively, for the upper curve.

signal from the burst position on timescales of 5 s, 10 s, 1000 s, or 3.4 hr, and in 2–10 or 2–28 keV. The  $3\sigma$  upper limit for the remainder of the observation, starting at 260 s after the trigger time, is  $1.7 \times 10^{-10}$  ergs  $\text{s}^{-1} \text{cm}^{-2}$  (2–10 keV; 3.6 ks net exposure time). This is a remarkable upper limit, see § 4. The  $3\sigma$  upper limit for all data obtained prior to 70 s before the trigger time is  $9 \times 10^{-11}$  ergs  $\text{s}^{-1} \text{cm}^{-2}$  (13.0 ks net exposure time).

### 3. THE X-RAY AFTERGLOW

The *BeppoSAX* Narrow-Field Instruments (NFI) consist of four devices, among them the Low-Energy (0.1 to 10 keV) and the Medium-Energy (2 to 10 keV) Concentrator Spectrometer (LECS and MECS, respectively; see Parmar et al. 1997 and Boella et al. 1997a, respectively). The NFI followed up on GRB 010222 from February 22.68 (8.0 hr after the burst) to February 25.01 UT (65 hr after the burst). The MECS was not turned on until 1.3 hr after the start. The net exposure time for the MECS is 88.4 ks and for the LECS 50.3 ks. The full-bandpass spatial MECS data were studied applying a maximum likelihood method (e.g., In 't Zand et al. 2000). Significant detections of four point sources were identified within  $10'$  from the WFC position (Fig. 3). A light curve of the brightest source (Fig. 4) shows a typical decay and unambiguously identifies the source with

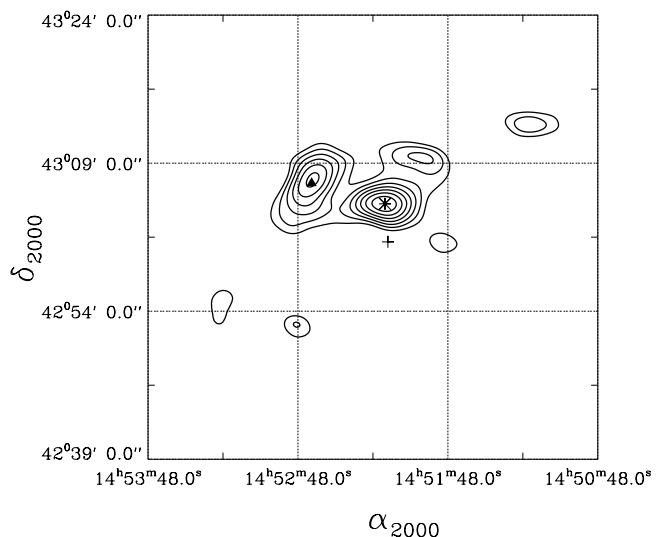


FIG. 3.—Contour map of detection significance in MECS data, after subtraction of the brightest source (the plus sign labels the best-fit position). Contours start at  $4\sigma$  and have steps of  $1\sigma$  for 1 dof. Three other sources are identified within  $10'$  from the afterglow, the two brightest are taken into account when generating light curves (Fig. 4) and spectra (Fig. 5). The best-fit positions of these are labeled with an asterisk and a triangle. Their positions are  $\alpha_{2000} = 14^{\text{h}}52^{\text{m}}13^{\text{s}}.2$ ,  $\delta_{2000} = +43^{\circ}04'52''.8$  and  $\alpha_{2000} = 14^{\text{h}}52^{\text{m}}42^{\text{s}}.5$ ,  $\delta_{2000} = +43^{\circ}07'7''.5$ . A similar map of the LECS data (not shown) reveals no sources other than the afterglow.

the X-ray afterglow of GRB 010222. The decay is consistent with a power-law function  $t^{-\alpha}$  ( $t$  time since GRB) with  $\alpha = 1.33 \pm 0.04$  ( $\chi^2_\nu = 1.01$  for  $\nu = 31$  dof). Such a decay index is very common for an X-ray afterglow. The flux at 8.0 hr of  $1.2 \times 10^{-11}$  ergs  $\text{s}^{-1} \text{cm}^{-2}$  is the brightest flux detected from any X-ray afterglow at the same epoch, except for GRB 991216 which was 3 times brighter (Takeshima et al. 1999). The position of the X-ray source is  $\alpha_{2000} = 14^{\text{h}}52^{\text{m}}12^{\text{s}}.0$ ,  $\delta_{2000} = +43^{\circ}01'01''.6$  (error radius  $30'$  at 90% confidence). This is  $7''$  from the X-ray position determined with the *Chandra X-ray Observatory* (*CXO*; Garmire et al. 2001) and  $8''$  from the optical transient (Henden 2001c; McDowell et al. 2001).

The overall energy spectrum could be modeled with an absorbed power law, with spectral index  $\beta = 0.97 \pm 0.05$  (again a very common value among X-ray afterglows) and  $N_{\text{H}} = (1.5 \pm 0.3) 10^{21} \text{cm}^{-2}$  ( $\chi^2_\nu = 0.83$  for  $\nu = 74$  dof, see Fig. 5).  $N_{\text{H}}$  is 1 order of magnitude smaller than during the prompt emission. Corrected for redshift,  $N_{\text{H}}$  is  $2.5 \times 10^{22} \text{cm}^{-2}$ . The 2–10 keV fluence of the afterglow, integrated over the observation span time, is 20 times smaller than that of the prompt emission. There is a small depression in the spectrum between 3 and 4 keV. We tested whether this feature is significant by modeling it with an absorption edge which is parameterized by a threshold energy  $E_{\text{edge}}$  and an optical depth  $\tau$ . We find that  $\chi^2_\nu$  improves to 0.79 for  $\nu = 72$ , with  $E_{\text{edge}} = 3.1 \pm 0.2$  keV and  $\tau = 0.19 \pm 0.10$ . An  $f$ -test predicts that the probability for a chance improvement is a marginal 0.7%. When corrected for redshift, the edge energy suggests K-edge absorption by Fe XIV–XVIII.

We searched the time-resolved and overall LECS + MECS spectrum for narrow emission features by resolving the data logarithmically in 10 time bins, and we were unable to find conclusive evidence. The  $3\sigma$  upper limit on a narrow line at 6 to 7 keV in the overall spectrum is

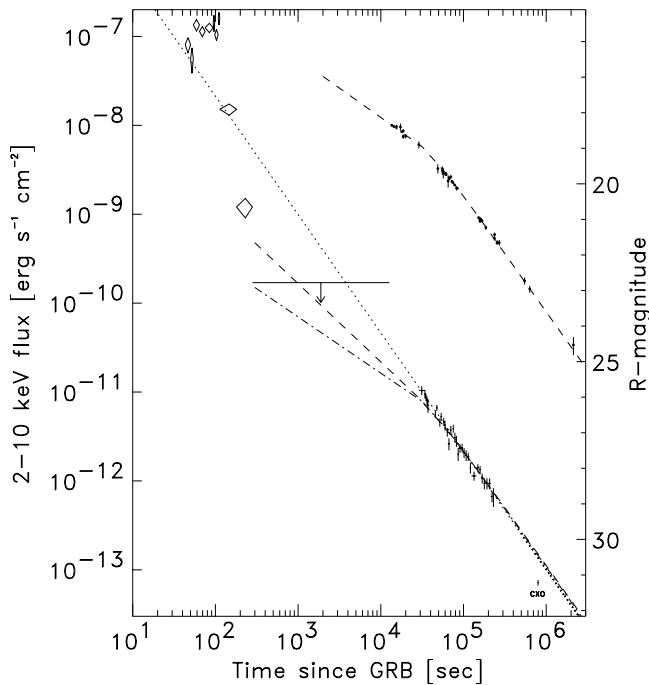


FIG. 4.—2–10 keV flux history (left ordinate) of the prompt emission (sole upper limit and diamonds whose sizes represent error margins) and afterglow emission (plus signs; based on MECS data, except for the first data point which is determined from LECS data and the last data point which is based on *CXO* data by Harrison et al. 2001b). A constant spectral shape was assumed throughout each data set to translate photon count rates to energy flux. The filled circles in top right-hand corner represent photometry in the Cousins *R* band (right ordinate) as taken and sometimes recalibrated from Stanek et al. (2001a, 2001b), Price et al. (2001), Orosz (2001), Masetti et al. (2001b), Oksanen et al. (2001), Stanek & Falco (2001), Valentini et al. (2001), Watanabe et al. (2001), Veillet (2001), and Garnavich et al. (2001b), together with the broken power-law fitted to these data (dashed curve) with a break time of  $41.5 \times 10^3$  s and decay indices  $\alpha$  of 0.60 before the break and 1.31 afterward (Masetti et al. 2001a). The same curve is also shown shifted to the level of the MECS data and taking  $\alpha$  before the break to be 0.85, as would be expected for adiabatic cooling. The dash-dotted curve shows the same function except that  $\alpha = 0.60$  before the break (to illustrate the case of radiative cooling). The dotted curve shows the best-fit power law function for the LECS/MECS data. All broken power laws fit the late WFC data better than the unbroken power law. However, for all power laws, the *CXO* data point (bottom right-hand corner) is a factor of 2 too faint with respect to the extrapolation of those.

$2 \times 10^{-6}$  photons  $\text{s}^{-1} \text{cm}^{-2}$ , at  $6.5/(1+z) = 2.6$  keV this is  $1.2 \times 10^{-5}$  photons  $\text{s}^{-1} \text{cm}^{-2}$ . For a Gaussian line with a width of 1 keV (FWHM) these upper limits are twice as high. The upper limit for the redshifted narrow line is similar to the flux of a  $3\sigma$  detection of a narrow line at 4.7 keV in GRB 000214 (Antonelli et al. 2000). With respect to the broad emission line detected in GRB 991216 at 3.5 keV (Piro et al. 2000), our upper limit is about 2 times smaller. We also studied, in the same 10 time bins, the 3.4–10 keV versus 1.8–3.4 keV hardness ratio and found no evidence for evolution in the continuum shape.

#### 4. DISCUSSION

For a redshift of  $z = 1.477$  (Jha et al. 2001a) and a  $\{H_0 = 65 \text{ km s}^{-1} \text{ Mpc}^{-1}, \Omega_m = 0.3, \Lambda = 0.7\}$  cosmology, the luminosity distance is  $D_L = 3.6 \times 10^{28}$  cm. If the emission is assumed to be isotropic, the  $\gamma$ -ray energy output is  $E_{\text{iso}}(\gamma) = 4\pi D_L^2 F_\gamma / (1+z)$  where  $F_\gamma$  is the observed fluence. In the 2–700 keV bandpass, this is  $7.7 \times 10^{53}$  ergs. In the redshift-corrected (or “comoving,” see Bloom, Frail & Sari

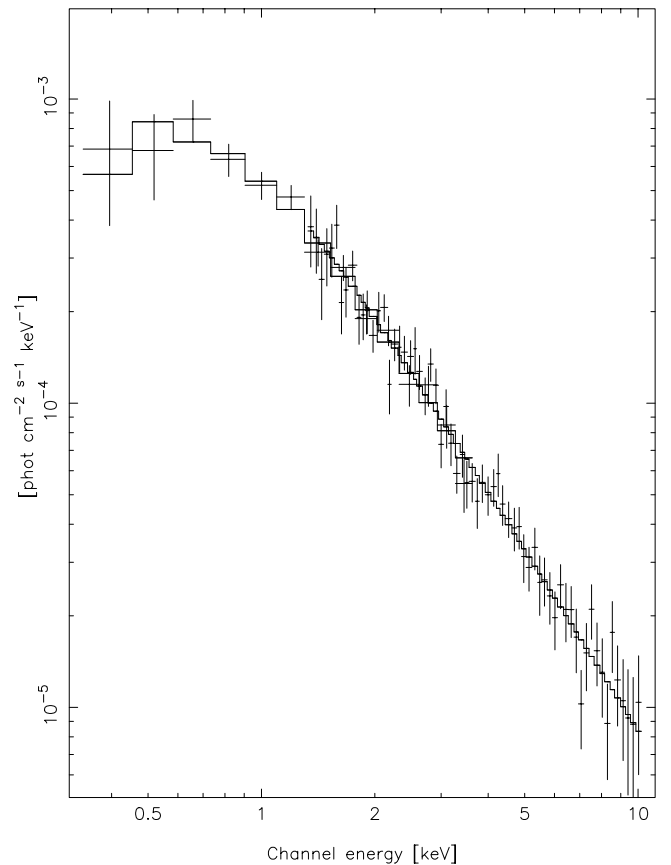


FIG. 5.—LECS and MECS spectral data for the whole observation and best-fit absorbed power-law function. The data were extracted through a maximum-likelihood fit to all point sources. This method retrieves all detected source photons. The LECS to MECS normalization was allowed to vary and converged to  $0.97 \pm 0.05$ .

2001b) 20–2000 keV bandpass, this is  $7.8 \times 10^{53}$  ergs. These two numbers are so close because the 20–2000 keV comoving band is close to the instrument band for the observer (8–807 keV). When compared to the 17 GRBs with established redshifts prior to GRB 010222 (Frail et al. 2001; Bloom et al. 2001b), there are only two other GRBs with higher values for  $E_{\text{iso}}(\gamma)$  in the comoving 20–2000 keV band: GRB 990123 (by a factor of 1.8) and GRB 000131 (by a factor of 1.5; this burst was not visible to *BeppoSAX*).

Optical photometry revealed an early break in the light curve (Holland et al. 2001), see Figure 4. Masetti et al. (2001a) carried out *UBVRIJK* photometry and determined that the break is achromatic. When fitted with a smoothed broken power law as defined by Beuermann et al. (1999), they find in the *R* band a break time of  $0.48 \pm 0.02$  days and decay indices of  $0.60 \pm 0.03$  and  $1.31 \pm 0.03$ , before and after the break. The *B*, *V*, and *I* light curves are convincingly consistent with the broken power law; the *J* and *K* bands are not sufficiently sampled to make a judgment. The slope change occurred relatively quickly; there is no difference with an unbroken power law from 1 day after the GRB on. The latest published *R*-band magnitude was obtained 25 days after the burst (Garnavich, Quinn, & Stanek 2001b) and is still consistent with the function parameterized by Masetti et al. (2001a).

Thanks to the long WFC coverage after the burst (3.5 hr) and the brightness of the prompt and afterglow emission, we are able to set significant constraints on the early X-ray

afterglow. While the NFI data are satisfactorily and accurately described by an unbroken power-law decay, the last two WFC data points lie significantly below the extrapolation of that power law (see Fig. 4). The one but last data point is  $5 \pm 1$  times fainter and the last data point, a  $3 \sigma$  upper limit, is  $1.5 \pm 0.1$  times fainter. Thus, a break is prescribed in X-rays. We have fitted the smoothed broken power-law function found by Masetti et al. (2001a) to the NFI data, leaving free only the normalization and employing  $\alpha = 0.60 + 0.25 = 0.85$  before the break, as would be expected for adiabatic cooling and for a cooling frequency between the X-ray and optical bands, and  $\alpha = 0.60$ , as would be expected for radiative cooling (Sari, Piran, & Narayan 1998), see Figure 4. Given that the afterglow is expected to begin during the main event (e.g., Frontera et al. 2000), these functions are more consistent with the late WFC data than the unbroken power law. We conclude that the X-ray data support the achromatic nature of the break seen in the optical. This is only the second time that a light curve break in a GRB afterglow is seen in X-ray data (Kuulkers et al. 2000; Pian et al. 2001). However, we note that the first three NFI data points are up to  $2 \sigma$  above the broken power-law functions. Furthermore, the preliminary X-ray flux as measured with *CXO* at 9 days after the burst by Harrison, Yost, & Kulkarni (2001b; see Fig. 4) lies  $48 \pm 6\%$  below the extrapolated unbroken power law and is similarly inconsistent with the broken power law. Therefore, the suggestion of the achromatic nature of the break is not as straightforward as one might hope.

In Figure 6, the optical photometry (Masetti et al. 2001a) and X-ray spectrum are shown for 0.97 days after the burst. Both data sets individually have similar spectral indices, but they do not match each other's extrapolations. The optical data are about 2.5 mag too faint or the X-ray data a factor of about 30 too bright. This cannot be explained by stan-

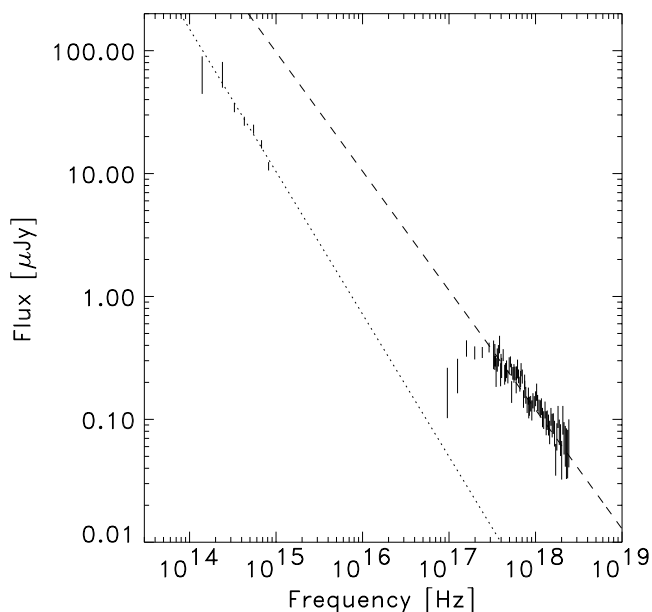


FIG. 6.—Broadband spectrum from *UBVRJK* photometry and X-ray spectrum at 0.97 days after the burst. The X-ray spectrum is for the whole NFI observation, but scaled to the flux level as observed at 0.97 days. No correction for absorption was carried out. The power-law functions fitted to each data set are shown (dotted line for optical data with spectral index 1.16 [Masetti et al. 2001a], and dashed line for X-ray data with spectral index 0.97).

dard extinction; possibly other extinction laws apply, as was already noted from absorption bands in the optical spectrum by Jha et al. (2001a) and Masetti et al. (2001a). Alternatively, the jump in the spectrum may be related to an important contribution to the X-ray spectrum of inverse Compton scattering while the optical spectrum is dominated by synchrotron emission (e.g., Sari & Esin 2001). This was recently suggested in a similar observation of another burst (Harrison et al. 2001a). Whatever the cause, the similar spectral indices indicate that there is no spectral break between the optical and X-ray bands. This is also consistent with the decay indices at these two wavelength regimes being equal (in fact, the X-ray decay index is the most accurate obtained for any GRB afterglow thus far and has a similarity to the optical decay index of  $2 \pm 4\%$ , which is the highest degree of agreement of all afterglows). This is in contrast to some other GRBs where the spectral break at the cooling frequency is between the optical and X-rays.

Currently, it is thought that two mechanisms may be responsible for achromatic breaks in GRB afterglows. In the first, the fireball has a collimated expansion (jet), and the break occurs when the bulk Lorentz factor becomes smaller than the inverse of the opening angle of the jet (Kulkarni et al. 1999; Sari, Piran, & Halpern 1999; Livio & Waxman 2000). Measurement of the break time directly provides the opening angle and the total amount of radiated energy. After the break,  $\alpha$  and  $\beta$  are related to the power-law index of the Lorentz-factor distribution of the electrons  $p$  through  $\alpha = p$  and  $\beta = p/2$ . The second mechanism concerns the deceleration of the fireball into the nonrelativistic (NR) domain in a dense circumburst medium (Dai & Lu 1999); the break occurs when the rest mass of the material swept up by the fireball equals the initial fireball energy. In this mechanism,  $\alpha = (3p - 4)/2$  and  $\beta = p/2$ . For the jet interpretation of the break, the two values for  $p$  determined from  $\alpha$  and  $\beta$  are  $1.33 \pm 0.03$  and  $1.93 \pm 0.10$ . The difference is  $5.7 \sigma$ , and the weighted mean 1.38. For the NR effect, the  $\alpha$ - and  $\beta$ -derived values for  $p$  are  $2.22 \pm 0.03$  and  $1.93 \pm 0.10$ . Here the difference is  $2.8 \sigma$  and the weighted mean 2.20. Clearly, the NR interpretation is favored over the jet interpretation because the difference between the two  $p$ -values is consistent with zero and the mean value of  $p$  is not smaller than 2, which would have implied an unbound energy estimate for the electrons. A similar conclusion was reached from optical observations alone by Masetti et al. (2001a). For the fireball to become nonrelativistic within 1 day after the burst, theory predicts (Blandford & McKee 1976) that, for an energy of  $\sim 10^{53}$  ergs (see below), a density for the circumburst medium of  $\sim 10^6 \text{ cm}^{-3}$  is required. The afterglow shows absorption equivalent to a redshift-corrected column density of  $\sim 10^{22} \text{ cm}^{-2}$ . Combining these two numbers implies a size of  $\sim 10^{16} \text{ cm}$ , or  $10^5 \text{ lt-s}$  for the dense part of the circumburst medium. This is large enough for the presumed fireball to be able to slow down to nonrelativistic speeds.

Given  $E_{\text{iso}}(\gamma) = 7.8 \times 10^{53}$  ergs (equivalent to  $0.4 M_{\odot}$  rest mass), it is likely that beaming is important in the initial stages of the burst, because no presently considered progenitor model is consistent with such a large energy (for similar arguments as applied to GRB 990123, see Kulkarni et al. 1999). However, there is no evidence in the data for a jet presence: one would have expected a steeper decay index that should also be larger than 2 before the NR-induced break (e.g., Livio & Waxman 2000; see also Piro et al. 2001,

where such behavior is shown for GRB 000926). Instead, the decay index is much shallower. The only way to make a jet “invisible” like that is to require that the jet-induced light-curve break happens simultaneously with the NR-induced one. From the formalism of Sari et al. (1999), and assuming an efficiency to convert energy to radiation of 1 and a density of  $\sim 10^6 \text{ cm}^{-3}$ , it follows that the opening angle  $\theta_j$  is of order  $15^\circ$ . The beaming-corrected energy is then  $3 \times 10^{52}$  ergs. This implies an unprecedentedly high energy content. However, this is uncertain, because it depends on whether early breaks in GRB 990123 and GRB 000131 are truly due to a jet (e.g., Dai & Lu 1999 for GRB 990123).

It should be noted that there is a consideration which favors a low-density interpretation of the observed light curve break. The jet opening angle for a mean circumburst density of  $0.1 \text{ cm}^{-3}$  is  $\theta_j = 2^\circ$ . Thus, the beaming-corrected energy output  $E_\gamma$  is  $(5.7 \pm 0.2) \times 10^{50}$  ergs. Frail et al. (2001) similarly apply a correction for beaming in 15 GRBs for which this is possible and find that  $E_\gamma$  has a range of  $0.234\text{--}1.80 \times 10^{51}$  ergs with a mean of  $5 \times 10^{50}$  ergs. This dynamic range is 3 times smaller than that of the uncorrected energies, which is compelling evidence that beaming is a dominant mechanism responsible for light curve breaks and that densities are low. For GRB 010222,  $E_\gamma$  happens to

be very close to the mean value for these 15 bursts (i.e., within 14%).

## 5. CONCLUSION

So far, GRB 010222 is the third most energetic GRB for which a distance has been determined. We measured the 2–10 keV light curve during the first 65 hr after the burst, except for a gap between 4 and 8 hr, and find that there is a break which is consistent with a break in the optical band. The jet-interpretation of this break is not straightforward, and an interpretation in the form of a quick brake of the fireball into a dense circumburst medium appears to be more consistent with the data. If this is indeed true, GRB 010222 may very well be the most energetic burst thus far detected.

We thank Elena Pian for her contribution to this work. Furthermore, we are grateful to the staff of the *BeppoSAX* Scientific Operation Center, the Mission Planning Team, and the Science Data Center for their support in obtaining and processing the data. J. Z. and E. K. acknowledge financial support from the Netherlands Organization for Scientific Research (NWO). The *BeppoSAX* satellite is a joint Italian and Dutch program.

## REFERENCES

- Amati, L., et al. 1997, *Proc. SPIE*, 3114, 176  
 Antonelli, A., et al. 2000, *ApJ*, 545, L39  
 Berger, E., & Frail, D. A. 2001, *GCN Circ.* 968 (<http://gcn.gsfc.nasa.gov/gcn/gcn3/968.gcn3>)  
 Beuermann, K., et al. 1999, *A&A*, 352, L26  
 Blandford, R. D., & McKee, C. F. 1976, *Phys. Fluids*, 19, 1130  
 Bloom, J. S., Djorgovski, S. G., Halpern, J. P., Kulkarni, S. R., Galama, T. J., Price, P. A., & Castro, S. M. 2001a, *GCN Circ.* 989 (<http://gcn.gsfc.nasa.gov/gcn/gcn3/989.gcn3>)  
 Bloom, J. S., Frail, D. A., & Sari, R. 2001b, *AJ*, 121, 2879  
 Boella, G., et al. 1997a, *A&AS*, 122, 327  
 Boella, G., Butler, R. C., Perola, G. C., Piro, L., Scarsi, L., & Bleeker, J. A. M. 1997b, *A&AS*, 122, 299  
 Dai, Z., & Lu, T. 1999, *ApJ*, 519, L155  
 Dickey, J. M., & Lockman, F. J. 1990, *ARA&A*, 28, 215  
 Di Paola, A., Antonelli, L. A., Li Causi, G., & Valentini, G. 2001, *GCN Circ.* 977 (<http://gcn.gsfc.nasa.gov/gcn/gcn3/977.gcn3>)  
 Feroci, M., et al. 1997, *Proc. SPIE*, 3114, 186  
 Feroci, M., Piro, L., Frontera, F., Torroni, V., Smith, M., Heise, J., & in 't Zand, J. 1999, *IAU Circ.* 7095  
 Fich, M., Phillips, R. R., Moriarty-Schieven, G., Tilanus, R. P. J., Frail, D. A., Smith, I. 2001, *GCN Circ.* 971 (<http://gcn.gsfc.nasa.gov/gcn/gcn3/971.gcn3>)  
 Frail, D. A., et al. 2001, *Nature*, submitted ([astro-ph/0102282](http://astro-ph/0102282))  
 Frontera, F., et al. 2000, *ApJ*, 540, 697  
 Frontera, F., et al. 2001, *ApJ*, 550, L47  
 Frontera, F., Costa, E., Dal Fiume, D., Feroci, M., Nicastro, L., Orlandini, M., Palazzi, E., & Zavattini, G. 1997, *A&AS*, 122, 357  
 Garmire, G. P., Garmire, A. B., Piro, L., & Schlegel, E. 2001, *GCN Circ.* 1005 (<http://gcn.gsfc.nasa.gov/gcn/gcn3/1005.gcn3>)  
 Garnavich, P. M., Pahre, M. A., Jha, S., Calkins, M., Stanek, K. Z., McDowell, J., & Kilgard, R. 2001a, *GCN Circ.* 965 (<http://gcn.gsfc.nasa.gov/gcn/gcn3/965.gcn3>)  
 Garnavich, P., Quinn, J., & Stanek, K. Z. 2001b, *GCN Circ.* 1009 (<http://gcn.gsfc.nasa.gov/gcn/gcn3/1009.gcn3>)  
 Harrison, F. A., et al. 2001a, *ApJ*, submitted ([astro-ph/0103377](http://astro-ph/0103377))  
 Harrison, F. A., Yost, S. A., & Kulkarni, S. R. 2001b, *GCN Circ.* 1023 (<http://gcn.gsfc.nasa.gov/gcn/gcn3/1023.gcn3>)  
 Henden, A., et al. 2001a, *GCN Circ.* 961 (<http://gcn.gsfc.nasa.gov/gcn/gcn3/961.gcn3>)  
 Henden, A., et al. 2001b, *GCN Circ.* 962 (<http://gcn.gsfc.nasa.gov/gcn/gcn3/962.gcn3>)  
 Henden, A., et al. 2001c, *GCN Circ.* 967 (<http://gcn.gsfc.nasa.gov/gcn/gcn3/967.gcn3>)  
 Holland, S., Fynbo, J., Gorosabel, J., Henden, A., Hjorth, J., Jensen, B., & Pedersen, H. 2001, *GCN Circ.* 1002 (<http://gcn.gsfc.nasa.gov/gcn/gcn3/1002.gcn3>)  
 In 't Zand, J. J. M., et al. 2000, *ApJ*, 545, 266  
 In 't Zand, J. J. M., Heise, J., van Paradijs, J., & Fenimore, E. E. 1999, *ApJ*, 516, L57  
 Jager, R., et al. 1997, *A&AS*, 125, 557  
 Jha, S., et al. 2001a, *ApJ*, 554, L155  
 Jha, S., Matheson, T., Calkins, M., Pahre, M. A., Stanek, K. Z., McDowell, J., Kilgard, R., & Garnavich, P. M. 2001b, *GCN Circ.* 974 (<http://gcn.gsfc.nasa.gov/gcn/gcn3/974.gcn3>)  
 Kulkarni, S. R., et al. 1999, *Nature*, 398, 389  
 Kuulkers, E., et al. 2000, *ApJ*, 538, 638  
 Livio, M., & Waxman, E. 2000, *ApJ*, 538, 187  
 Masetti, N., et al. 2001a, *A&A*, 374, 382  
 Masetti, N., Palazzi, E., Pian, E., Zacchei, A., Magazzu, A., Pedani, M., Ghinassi, F., & Mignoli, M. 2001b, *GCN Circ.* 985 (<http://gcn.gsfc.nasa.gov/gcn/gcn3/985.gcn3>)  
 McDowell, J., Kilgard, R., Garnavich, P. M., Stanek, K. Z., & Jha, S. 2001, *GCN Circ.* 963 (<http://gcn.gsfc.nasa.gov/gcn/gcn3/963.gcn3>)  
 Morrison, R., & McCammon, D. 1983, *ApJ*, 270, 119  
 Oksanen, A., Moilanen, M., Hyvonen, R., Pasanen, R., & Tikkanen, P. 2001, *GCN Circ.* 990 (<http://gcn.gsfc.nasa.gov/gcn/gcn3/990.gcn3>)  
 Orosz, J. A. 2001, *GCN Circ.* 976 (<http://gcn.gsfc.nasa.gov/gcn/gcn3/976.gcn3>)  
 Parmar, A. N., et al. 1997, *A&AS*, 122, 309  
 Pian, E., et al. 2001, *A&A*, 372, 456  
 Piro, L. 2001, *GCN Circ.* 959 (<http://gcn.gsfc.nasa.gov/gcn/gcn3/959.gcn3>)  
 Piro, L., et al. 2000, *Science*, 290, 955  
 Piro, L., et al. 2001, *ApJ*, in press ([astro-ph/0103306](http://astro-ph/0103306))  
 Price, P. A., Gal-Yam, A., Ofek, E., Yost, S., Bloom, J. S., Galama, T. J., Harrison, F., & Kulkarni, S. R. 2001, *GCN Circ.* 973 (<http://gcn.gsfc.nasa.gov/gcn/gcn3/973.gcn3>)  
 Sari, R., & Esin, A. A. 2001, *ApJ*, 548, 787  
 Sari, R., Piran, T., & Halpern, J. P. 1999, *ApJ*, 519, L17  
 Sari, R., Piran, T., & Narayan, R. 1998, *ApJ*, 497, L17  
 Stanek, K. Z., Challis, P., Jha, S., Kilgard, R., McDowell, J., & Garnavich, P. 2001a, *GCN Circ.* 983 (<http://gcn.gsfc.nasa.gov/gcn/gcn3/983.gcn3>)  
 Stanek, K. Z., & Falco, E. 2001, *GCN Circ.* 991 (<http://gcn.gsfc.nasa.gov/gcn/gcn3/991.gcn3>)  
 Stanek, K. Z., Jha, S., McDowell, J., Kilgard, R., Roll, J., Garnavich, P. M., & Kaluzny, J. 2001b, *GCN Circ.* 970 (<http://gcn.gsfc.nasa.gov/gcn/gcn3/970.gcn3>)  
 Stornelli, M., Celidonio, F., Muller, J. M., In 't Zand, J., Amati, L., Feroci, M., & Gandolfi, G. 2000, *GCN Circ.* 540 (<http://gcn.gsfc.nasa.gov/gcn/gcn3/540.gcn3>)  
 Takeshima, T., Markwardt, C., Marshall, F., Giblin, T., & Kippen, R. M. 1999, *GCN Circ.* 478 (<http://gcn.gsfc.nasa.gov/gcn/gcn3/478.gcn3>)  
 Tavani, M. 1996, *Phys. Rev. Lett.*, 76, 3478  
 Valentini, G., Massi, F., Dolci, M., & Di Carlo, E. 2001, *GCN Circ.* 992 (<http://gcn.gsfc.nasa.gov/gcn/gcn3/992.gcn3>)  
 Veillet, C. 2001, *GCN Circ.* 1000 (<http://gcn.gsfc.nasa.gov/gcn/gcn3/1000.gcn3>)  
 Watanabe, J.-I. et al. 2001, *GCN Circ.* 993 (<http://gcn.gsfc.nasa.gov/gcn/gcn3/993.gcn3>)